Open Access Online Journal on Astronomy and Astrophysics

Acta Astrophysica Taurica

www.astrophysicatauricum.org

Acta Astrophys. Tau. 6(1), 24–30 (2025)

Full electric current in active regions with different levels of flare productivity: first results

Yu.A. Fursyak

Crimean Astrophysical Observatory, Nauchny 298409
e-mail: yuriy_fursyak@mail.ru

Received 2 October 2024

ABSTRACT

The study aims to analyze the magnitude and dynamics of the full electric current, as well as its components – the vertical and horizontal electric currents – in active regions (ARs) with different levels of flare productivity. To calculate the magnitude of the electric current, we used data from the Helioseismic and Magnetic Imager (HMI) on board the Solar Dynamics Observatory (SDO) on the spatial distribution of the magnetic field vector components at the level of the solar photosphere. Twelve ARs were studied: three ARs with low, three ARs with moderate, and six ARs with high flare productivity. Each AR was monitored within 30–35 degrees relative to the central solar meridian, which corresponds to a time interval of 3–5 days. The preliminary results are as follows: (1) In most of the considered cases, the average unsigned density of the horizontal electric current is 1.5–4.5 times greater than the density of the vertical electric current; the magnitude of the full electric current is thus determined mainly by the horizontal electric current. (2) In NOAA AR 11283 and 12297, the time intervals of several tens of hours were revealed; within these intervals the average unsigned density of the vertical electric current is approximately equal to or greater than the average unsigned density of the horizontal electric current. (3) In NOAA AR 11158 and 12673 of the analyzed sample, in which the emergence of new magnetic fluxes was recorded during the monitoring time, an increase in the magnitudes of the vertical, horizontal, and full electric currents is observed 18–20 hours before the first solar flares of high X-ray classes; the time of increase in the electric current is significantly less than the time interval of increase in the magnitude of the total unsigned magnetic flux. (4) There is no explicit relationship between the magnitude of the full electric current and the flare productivity of an AR determined by the flare index. (5) The highest absolute values of the full electric current density are characteristic of ARs with moderate flare productivity.

Key words: Sun, solar activity, active regions, electric currents

1 Introduction

Electric currents play a significant role in the evolution of active regions (ARs). In the early work of Alfven, Carlquist (1967), it was noted that "the description of a series of processes in the solar atmosphere in terms of the electric current is often more interesting than in terms of the magnetic field."

The full electric current has two components: vertical and horizontal. The vertical electric current is easier to calculate: it requires data on the transverse magnetic field at a given level of the solar atmosphere. There are two approaches to calculating the vertical current: the differential method, which can be considered classical as it was used in the early studies of electric currents in the solar atmosphere (see, e.g., Severnyi, 1965); and the integral method, which began to be applied in the 1980s (Abramenko, Gopasyuk, 1987).

The situation is significantly worse for calculating the horizontal electric current, as it requires information about the vertical component of the magnetic field at two levels of the solar atmosphere. Although dual-channel magnetographs were developed in their time (Stepanov, Severny, 1962; Ioshpa, Mogilevskii, 1965; Kuznetsov et al., 1966; Severny, 1966; Livingston, 1968), they have not been widely adopted to this day. Moreover, systematic measurements of magnetic fields at two heights with good temporal and spatial resolution are entirely absent. This makes it impossible to directly calculate the horizontal electric current using observations in two spectral lines formed at different heights, as was done in the 1960s and 1970s (see, e.g., Kotov, 1970, 1971). Consequently, alternative and often indirect methods for calculating the horizontal current must be sought. For example, Hofmann and Staude (1987) estimated the azimuthal component of the electric current by assuming a specific geometry of a highly inclined magnetic flux tube forming an isolated sunspot. Pevtsov and Peregud (1990) assumed azimuthal (cylindrical) symmetry to derive three components of the electric current. In the late 1990s, Chinese astronomers proposed a rather interesting method for estimating horizontal electric currents. Their approach uses real vector magne-

tograms at one level of the solar atmosphere, which serve as boundary conditions for calculating the magnetic field vector components at the second level (Ji et al., 1998). A method for calculating the horizontal current was also proposed by Abramenko (2008). In this case, by considering a thin layer and applying straightforward mathematical calculations and some assumptions, it is possible to estimate horizontal currents in the solar photosphere. This method was later refined and tested (Fursyak, Abramenko, 2017). It is this approach that is used in this work to calculate the horizontal electric current. It should be noted that the values of horizontal electric current density obtained using the above methods are in good agreement with each other not only by order of magnitude but are close in absolute values, and they correlate with the results of earlier works (e.g., Kotov, 1970).

This work aims to study the dynamics of the full electric current and its components (vertical and horizontal currents) and to identify patterns and features of the temporal variations of the electric current in regions with different levels of flare productivity. Given the current lack of systematic measurements of horizontal electric currents and, consequently, the inability to study their dynamics, as well as the dynamics of the full electric current, the tasks addressed here represent a new direction of research, and the presented results are unique in their kind.

2 Data

The main body of the work (calculation of magnetic field parameters and electric currents) is based on magnetographic data from the Helioseismic and Magnetic Imager (HMI, Scherrer et al., 2012) on board the Solar Dynamics Observatory (SDO, Pesnell et al., 2012). We used the Space-Weather HMI Active Region Patches (SHARP, Bobra et al., 2014) magnetograms of the magnetic field vector components at the level of the solar photosphere in cylindrical coordinates with a temporal resolution of 12 minutes and a spatial resolution of 0.5″ pixel^{-1} (data series hmi.sharp_cea_720s), available on the Joint Science Operations Center (JSOC) website[1]. Along with magnetographic data from the JSOC website, we additionally downloaded a bitmap mask (allowing the selection of an AR with a unique National Oceanic and Atmospheric Administration, NOAA, identifier on a rectangular SHARP magnetogram) and a conf_disambig mask (allowing the selection of pixels on the magnetogram where the π-ambiguity of the azimuth of the transverse magnetic field has been resolved with high confidence).

To plot graphs exhibiting the dynamics of the X-ray flux in the 1–8 Å range in Earth's orbit, we additionally used data from the GOES-15 spacecraft[2], as well as data from the catalog of the magneto-morphological classification (MMC) of ARs[3] developed by Abramenko et al. (2018) at the Crimean Astrophysical Observatory and modified in 2021 (Abramenko, 2021), which, in addition to information about the type of an AR, also contains data on the most powerful flares recorded in the region and its flare index.

3 Targets

We examined 12 ARs of solar cycle 24. The basic parameters of the studied regions are presented in Table 1. The second column of the table lists the region number according to the NOAA classification; the third column shows the monitoring time of an AR (corresponding to the time interval during which the region was within ±35° relative to the central solar meridian). The fourth column provides the time-averaged value of the total unsigned magnetic flux (averaging over time is denoted by an overline). The total unsigned magnetic flux of an AR was calculated using the formula $\Phi = s_{\rm pix} \times \sum |B_z|_{\rm bitmap+575}$, where $s_{\rm pix}$ is the pixel area on the HMI/SDO magnetogram, and $\sum |B_z|_{\rm bitmap+575}$ is the sum of the absolute values of the magnetic field strengths at a

[1] http://jsoc2.stanford.edu/ajax/lookdata.html
[2] https://www.ncei.noaa.gov/data/goes-space-environment-monitor/access/full/
[3] https://sun.crao.ru/databases/catalog-mmc-ars

Table 1. Basic parameters of the analyzed ARs.

№	AR number (NOAA)	Monitoring time	$\overline{\Phi}$, 10^{22} Mx	AR type (MMC)	Most powerful flare	Flare index (FI)	$< \overline{\lvert j_z \rvert} >$, mA m^{-2}	$< \overline{\lvert j_\perp \rvert} >$, mA m^{-2}	$< \overline{\lvert J \rvert} >$, mA m^{-2}
1	2	3	4	5	6	7	8	9	10
1	11158	12-15.02.2011	0.76	B2	X2.2 15.02.2011	59.26	4.10	7.07	8.18
2	11283	04-07.09.2011	0.39	B2	X2.1 06.09.2011	45.61	3.12	3.99	5.10
3	11302	27-30.09.2011	1.49	A2	X1.9 24.09.2011	78.79	3.53	6.57	7.47
4	11711	04-07.04.2013	0.29	A1	C1.7 03.04.2013	0.17	2.35	5.50	5.99
5	11890	07-10.11.2013	1.48	A2	X3.3 05.11.2013	55.63	3.23	9.88	10.40
6	12297	11-14.03.2015	0.83	B3	X2.2 11.03.2015	46.32	4.62	4.40	6.43
7	12305	25-29.03.2015	1.08	B1	C8.7 25.03.2015	1.33	2.69	4.84	5.57
8	12339	10-13.05.2015	2.17	B2	M1.9 06.05.2015	8.80	2.83	6.86	7.43
9	12443	02-05.11.2015	1.87	B2	M3.7 04.11.2015	11.84	2.78	12.40	12.71
10	12473	25-30.12.2015	1.20	B2	M4.7 23.12.2015	9.02	2.89	9.19	9.65
11	12673	02-05.09.2017	0.92	B3	X9.3 06.09.2017	223.83	3.99	8.75	9.63
12	12674	03-06.09.2017	1.40	A1	C5.2 30.08.2017	0.76	2.49	4.76	5.38

level of > 575 G (see Norton et al., 2017) within the bitmap mask. The fifth column of the table indicates the region type according to the MMC, where regions are divided into three main types: U – unipolar, A – regions that follow the basic empirical patterns established for sunspot groups, and B – regions that violate the basic empirical patterns established for sunspot groups. In the analyzed sample, there are no regions of type U, four regions of type A, and eight regions of type B. The sixth column of the table contains information about the X-ray class of the most powerful flare recorded in the studied AR and the date on which it was recorded. It is by the maximum X-ray class of flares recorded in the AR during its presence on the visible solar disk that its flare productivity is determined here. Low flare productivity implies the recording of only C flares; moderate productivity, the recording of C and M flares; and high productivity, the recording of at least one X flare in the AR, in addition to others. The seventh column shows the value of the flare index (FI) of an AR (Abramenko, 2005): $\mathrm{FI} = \frac{1}{\tau} \times (\sum \mathrm{C} + 10 \sum \mathrm{M} + 100 \sum \mathrm{X})$, where τ is the time (in days) the AR is on the visible solar disk; $\sum \mathrm{C}$, $\sum \mathrm{M}$, $\sum \mathrm{X}$ are the total importance of flares of X-ray classes C, M, and X, respectively, recorded in the AR. The flare index of an AR will be 1.0 (100.0) if one flare of X-ray class C1.0 (X1.0) is recorded daily in the AR. The analyzed sample includes three ARs with low flare productivity (NOAA AR 11711, 12305, and 12674), three ARs with moderate flare productivity (NOAA AR 12339, 12443, and 12473), and six ARs with high flare productivity, three of which (NOAA AR 11158, 11283, and 12673) had evolutionary features during their monitoring time (emergence of a new magnetic flux or intense movements of individual sunspots in a group). As can be seen from the data in Table 1, the flare index of ARs with low flare productivity does not exceed a few units, that of ARs with moderate productivity reaches values of about ten units, and that of ARs with high flare productivity has values of several tens of units, and in some cases (NOAA AR 12673) several hundred. Columns 8–10 of the table contain information about the average unsigned values of the density of the vertical, horizontal, and full electric currents in the AR, averaged over the monitoring time (4–5 days with a cadence of 12 minutes, i.e., averaging over time is performed over 400–600 points). More details about these parameters are provided in Sections 4 and 5.

4 Methods for calculating analyzed parameters

As noted in Introduction, to calculate the full electric current, it is necessary to know the values of its components – the vertical and horizontal currents.

There are two methods for calculating the vertical electric current: differential and integral. Here, the integral method is used. It is described in detail in Fursyak (2018). The approach is based on the integral form of the Ampère law:

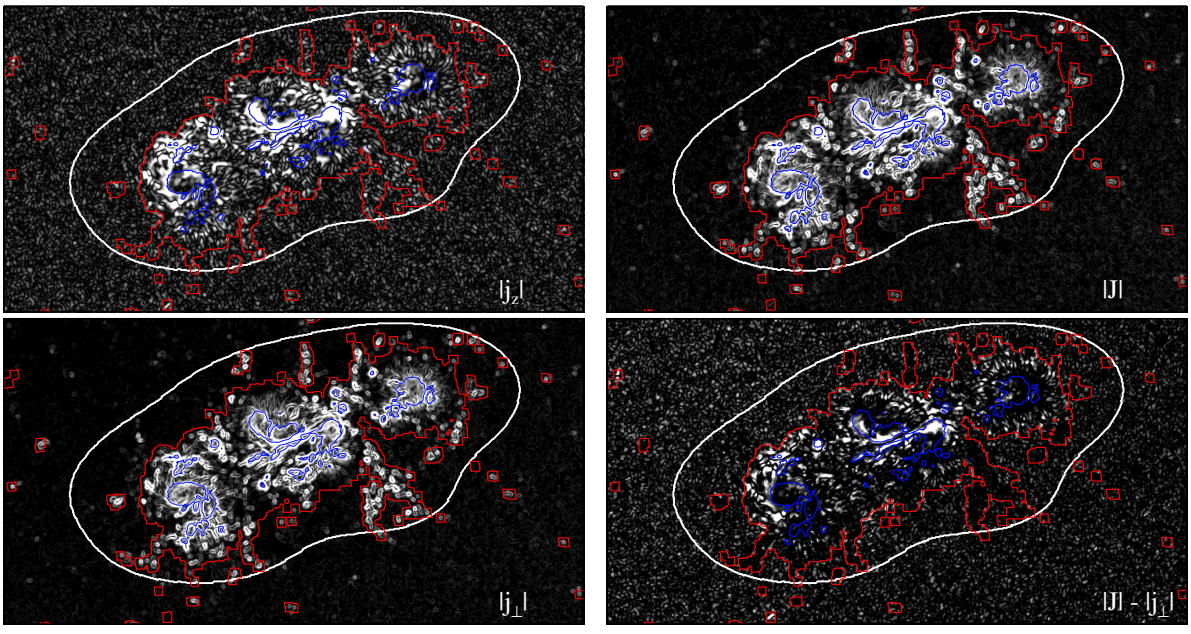

AR NOAA 11158 00:00UT 15.02.2014

Fig. 1. Maps of the distribution of the modulus of the vertical (top left), horizontal (bottom left), and full (top right) electric current density in NOAA AR 11158 at 00:00 UT on February 15, 2011 (approximately two hours before the X2.2 flare). The bottom right panel shows a map of the difference between the values of the horizontal and full electric current density. The maps are scaled as follows: top left – from 0 (black) to 0.01 A m^{-2} (white), bottom left and top right – from 0 (black) to 0.04 A m^{-2} (white), bottom right – from 0 (black) to 0.005 A m^{-2} (white). The white contour denotes the bitmap mask; the red contour, the conf_disambig mask. Blue contours denote sunspots in the AR with an absolute magnetic field strength of more than 1000 G. The image scale is 270 × 137 Mm.

$$(I_z)_{i,j} = \frac{1}{\mu_0}\int_L \boldsymbol{B}_t\, dr, \qquad (1)$$

where $\mu_0 = 4\pi \times 10^{-7}$ H m^{-1} is the magnetic constant; $\boldsymbol{B}_t \equiv (B_x, B_y)$ is the vector of the transverse magnetic field of an AR; dr is the integration element, equal in magnitude to the pixel size on the HMI/SDO magnetogram (363 km); i and j are the coordinates of the pixel on the magnetogram where the value of the vertical electric current is calculated. The integral on the right side of expression (1) is calculated approximately using Simpson's method. The integration contour L has a rectangular shape and dimensions of 5×5 pixels. Averaging the current over the area of the contour L gives the value of the vertical current density in its central pixel $(j_z)_{i,j}$.

The calculation of the horizontal electric current is performed using the method described in Fursyak, Abramenko (2017). The primary formula is Ampère's law in differential form:

$$\mu_0 \boldsymbol{j} = \nabla \times \boldsymbol{B}, \qquad (2)$$

and the final formula for estimating the square of the horizontal electric current density is

$$j_\perp^2 = \frac{1}{\mu_0^2}\left[\left(\frac{\partial B_z}{\partial x}\right)^2 + \left(\frac{\partial B_z}{\partial y}\right)^2\right]. \qquad (3)$$

As can be seen, expression (3) allows only the absolute value of the horizontal electric current density vector to be determined, but not its direction. Thus, the direction of the full electric current vector also cannot be determined. However, it is possible to calculate the full electric current density, knowing the values of the vertical and horizontal current density in each pixel of the original magnetogram:

$$J = \sqrt{(j_z)^2 + (j_\perp)^2}. \qquad (4)$$

Examples of maps of the distribution of absolute values of the horizontal, vertical, and full electric current density, as well as a map of the difference between the full and horizontal current density, are shown in Fig. 1.

5 Results

Based on the obtained maps of the vertical, horizontal, and full electric current density distributions, the average unsigned densities of the vertical $< |j_z| >$, horizontal $< |j_\perp| >$, and full $< |J| >$ currents were calculated for all regions of the analyzed sample. Temporal variations of the electric current parameters were plotted for each AR over the monitoring time. Examples of these plots are shown in Fig. 2 (typical cases are presented).

As seen from the presented plots, the average unsigned vertical electric current density $< |j_z| >$ significantly differs for ARs with different levels of flare productivity: higher values of this parameter are characteristic of ARs with higher flare productivity. Meanwhile, similar behavior is not observed for the average unsigned horizontal and full electric current densities. Thus, it can be concluded that the vertical electric current is associated with flares in ARs, whereas the horizontal current is involved in other processes.

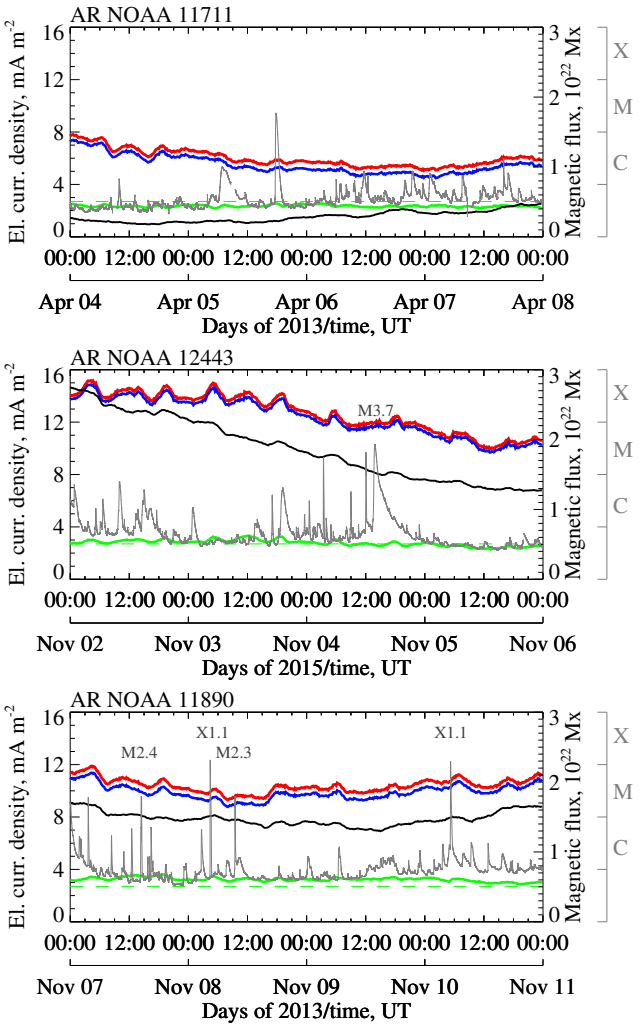

Fig. 2. Dynamics of the average unsigned density of the vertical (green curve), horizontal (blue curve), and full (red curve) electric currents in ARs with low (top), moderate (center), and high (bottom) flare productivity. The black curve shows the dynamics of the total unsigned magnetic flux of ARs; the gray curve, the solar X-ray flux in the 1–8 Å range at the Earth orbit (according to GOES-15 data). The X-ray classes of the most powerful flares recorded in the studied ARs are indicated. Typical cases are presented.

It is also evident from the plots in Fig. 2 that the horizontal current density is 1.5–4.5 times greater than the corresponding vertical current density values. Thus, the horizontal current contributes predominantly to the absolute values of the full electric current. However, in the analyzed sample of ARs, for two cases (see Fig. 3) – NOAA AR 11283 and 12297 – we found time intervals during which the average unsigned vertical electric current density is approximately equal to or even greater than the average unsigned horizontal current density. For NOAA AR 11283, this time interval is approximately 35 hours, while for NOAA AR 12297, it is 64 hours. The current data volume is insufficient to draw any

conclusions, but if a similar pattern is observed in a larger dataset, it will be necessary to further investigate such ARs.

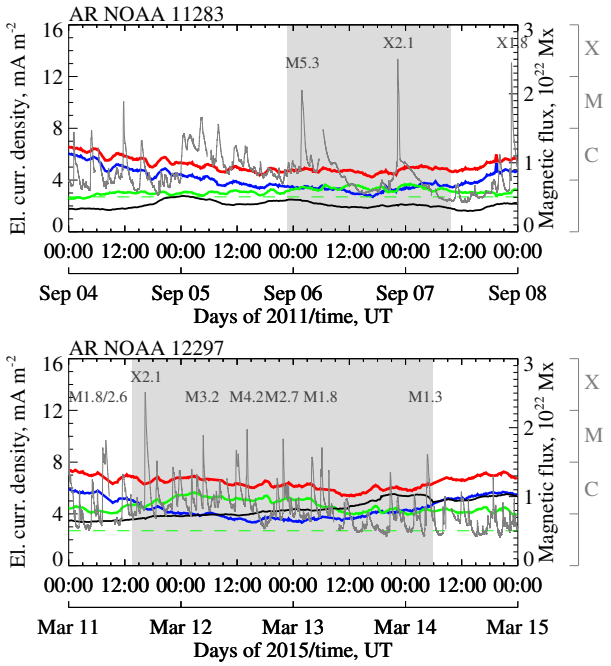

Fig. 3. Dynamics of electric current parameters in NOAA AR 11283 (top) and 12297 (bottom). The notation is the same as in Fig. 2. The gray shaded area marks the time interval during which the average unsigned vertical electric current density is approximately equal to or greater than the average unsigned horizontal current density.

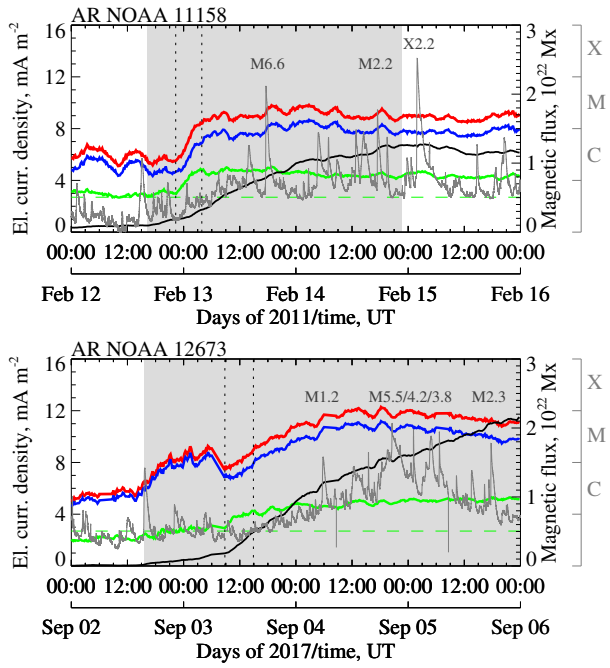

Fig. 4. Dynamics of electric current parameters in NOAA AR 11158 (top) and 12673 (bottom) with additional magnetic flux emergence. The notation is the same as in Fig. 2. The gray shaded area marks the time interval of the total unsigned magnetic flux increase, and the vertical dashed lines indicate the time interval of rapid increase in the average unsigned vertical electric current density above the critical value (2.7 mA m^{-2}).

The dynamics of electric current parameters in NOAA AR 11158 and 12673, where additional magnetic flux emergence was observed during the monitoring time (see Fig. 4), are of particular interest. First, it is important to note significant fluctuations in the horizontal and full electric current densities even before the onset of magnetic flux emergence. In NOAA AR 11158, these fluctuations are detected as early as 16 hours before the magnetic flux emergence, while in NOAA AR 12673, they are observed approximately two hours before. Meanwhile, no significant changes in the average unsigned vertical electric current density are observed during these time intervals. A substantial and relatively rapid increase in $< |j_z| >$ above the critical value of 2.7 mA m^{-2} (see Fursyak et al., 2020) begins in NOAA AR 11158 approximately six hours after the onset of magnetic flux emergence, while in NOAA AR 12673, it starts 17 hours later, lasting about six hours in both cases (this time interval is marked by vertical dashed lines in Fig. 4). This may indicate a rapid redistribution of magnetic energy in the ARs. Almost simultaneously (with a delay of no more than an hour), an increase in $< |j_\perp| >$ and $< |J| >$ begins, but the rise time for these parameters is longer (approximately ten hours for NOAA AR 11158 and more than a day for NOAA AR 12673). These results further support the earlier suggestion that the components of the full electric current – the horizontal and vertical currents – are associated with different processes in the solar atmosphere. It should also be noted that the increase in the average unsigned vertical, horizontal, and full electric current densities is detected approximately 18–20 hours before the first flares of high X-ray classes, and that the growth of the total unsigned magnetic flux in the ARs occurs on a significantly longer timescale than the growth of the electric current parameters.

Table 2. Average values of the flare index (FI) and electric current parameters for regions with different levels of flare productivity.

	<FI>	$<< \overline{\lvert j_z \rvert} >>$, mA m^{-2}	$<< \overline{\lvert j_\perp \rvert} >>$, mA m^{-2}	$<< \overline{\lvert J \rvert} >>$, mA m^{-2}
1	2	3	4	5
Regions with low flare productivity	0.75	2.51	5.03	5.65
Regions with moderate flare productivity	9.89	2.83	9.48	9.93
Regions with high flare productivity	84.91	3.77	6.78	7.87

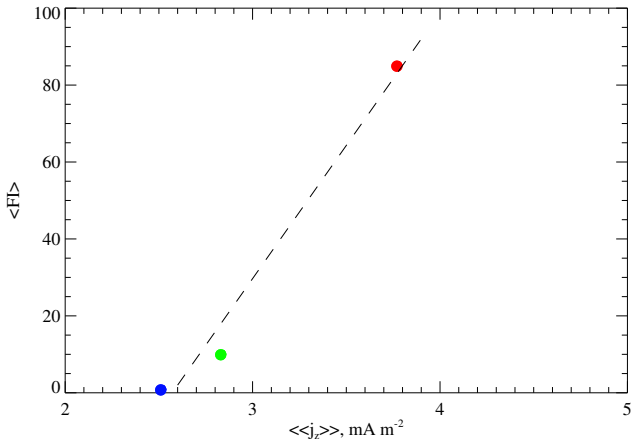

Fig. 5. Relationship between the averaged mean unsigned vertical electric current density << $\overline{|j_z|}$ >> and the average flare index (<FI>) for regions with low (blue dot), moderate (green dot), and high (red dot) flare productivity.

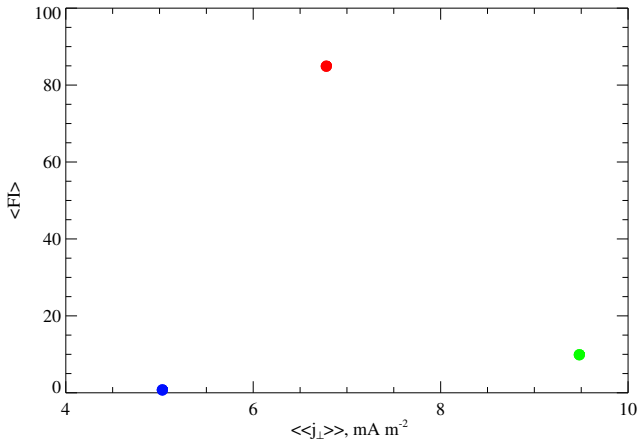

Fig. 6. Relationship between the averaged mean unsigned horizontal electric current density << $\overline{|j_\perp|}$ >> and the average flare index (<FI>). The notation is the same as in Fig. 5.

Averaging the analyzed electric current parameters over regions with low (NOAA AR 11711, 12305, 12674), moderate (NOAA AR 12339, 12443, 12473), and high (NOAA AR 11158, 11283, 11302, 11890, 12297, 12673) flare productivity revealed the following (see Table 2 and Figs. 5–7):

- The relationship between the averaged mean unsigned vertical electric current density << $\overline{|j_z|}$ >> and the average flare index (<FI>), shown in Fig. 5, is quasi-linear: the greater the vertical electric current, the higher the flare productivity of an AR.
- The relationship between the averaged mean unsigned horizontal electric current density << $\overline{|j_\perp|}$ >> and the average flare index (<FI>) is significantly more complex (see Fig. 6). It is evident that for ARs in the analyzed sample with moderate flare productivity, the value of << $\overline{|j_\perp|}$ >> is almost 1.5 times greater than for regions with high flare productivity. However, this may be due to a selection effect: the analyzed sample itself is small. The observed effect might be explained by the complexity of the magnetic configuration of ARs: as follows from the data in Table 1, the regions selected for analysis with moderate activity belong to type B2 according to the MMC, i.e., they violate the main empirical patterns established for sunspot groups.
- The relationship between the averaged mean unsigned full electric current density << $\overline{|J|}$ >> and the average flare index (<FI>) is similar to that for the pair << $\overline{|j_\perp|}$ >> – <FI> (Fig. 7). This is explained by the fact that, as mentioned earlier, the mean unsigned horizontal electric current density in most cases exceeds the mean unsigned vertical current density, and thus, this parameter contributes predominantly to the full electric current density.

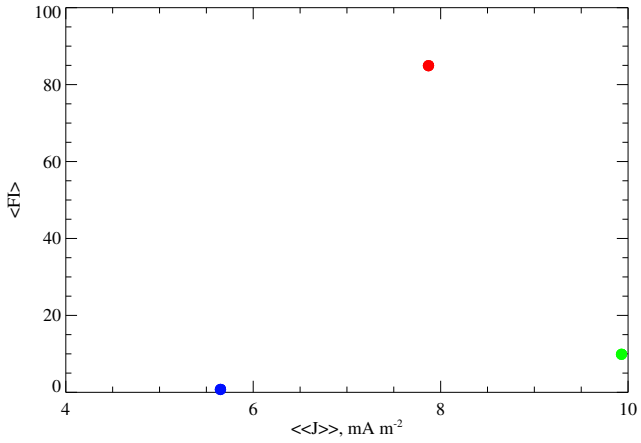

Fig. 7. Relationship between the averaged mean unsigned full electric current density << $\overline{|J|}$ >> and the average flare index (<FI>). The notation is the same as in Fig. 5.

6 Conclusions

The study of the dynamics of the vertical, horizontal, and full electric currents in a small sample of 12 ARs from solar cycle 24 reveals several features that require further statistical investigation for confirmation:

1. In most cases examined, the average unsigned density of the horizontal electric current is 1.5–4.5 times greater than the density of the vertical electric current. Thus, the magnitude of the full electric current is predominantly determined by the horizontal electric current.
2. In two cases (NOAA AR 11283 and 12297), time intervals were identified during which the average unsigned density of the vertical electric current was approximately equal to or greater than the average unsigned density of the horizontal electric current. For NOAA AR 11283,

this time interval was 35 hours, and for NOAA AR 12297, it was 64 hours.
3. In NOAA AR 11158 and 12673 from the analyzed sample, with the emergence of new magnetic fluxes during the monitoring time, an increase in the magnitudes of the vertical, horizontal, and full electric currents was detected 18–20 hours before the first flares of high X-ray classes. The rise time of the electric current is significantly shorter than the time interval of the increase in the total unsigned magnetic flux.
4. No clear correlation was found between the magnitude of the full electric current and the flare productivity of the ARs determined by the flare index.
5. The highest absolute values of the full electric current density were recorded in ARs with moderate flare productivity.

Acknowledgments. This work was supported by the Russian Ministry of Education and Science, state assignment No. 122022400224-7. The author thanks the referee for interest and valuable comments, which significantly helped to improve the manuscript.

References

Abramenko V.I., 2005. Astrophys. J., vol. 629, iss. 2, pp. 1141–1149.
Abramenko V.I., 2008. arXiv:0806.1547.
Abramenko V.I., 2021. Mon. Not. Roy. Astron. Soc., vol. 507, iss. 3, pp. 3698–3706.
Abramenko V.I., Gopasyuk S.I., 1987. Izv. Krymsk. Astrofiz. Observ., vol. 76. pp. 147–168. (In Russ.)
Abramenko V.I., Zhukova A.V., Kutsenko A.S., 2018. Geomagnetism and Aeronomy, vol. 58, iss. 8, pp. 1159–1169.
Alfven H., Carlquist P., 1967. Solar Phys., vol. 1, iss. 2, pp. 220–228.
Bobra M.G., Sun X., Hoeksema J.T., et al., 2014. Solar Phys., vol. 289, iss. 9, pp. 3549–3578.
Fursyak Yu.A., 2018. Geomagnetism and Aeronomy, vol. 58, iss. 8, pp. 1129–1135.
Fursyak Yu.A., Abramenko V.I., 2017. Astrophysics, vol. 60, iss. 4, pp. 544–552.
Fursyak Yu.A., Abramenko V.I., Kutsenko A.S., 2020. Astrophysics, vol. 63, iss. 2, pp. 260–273.
Hofmann A., Staude J., 1987. Publications of the Astronomical Institute of the Czechoslovak Academy of Sciences, vol. 66, pp. 105–107.
Ioshpa B.A., Mogilevskii E.I., 1965. Soln. aktivnost', no. 2, pp. 118–130. (In Russ.)
Ji H.S., Song M.T., Li X.Q., Hu F.M., 1998. Solar Phys., vol. 182, iss. 2, pp. 365–379.
Kotov V.A., 1970. Izv. Krymsk. Astrofiz. Observ., vol. 41–42, pp. 67–88. (In Russ.)
Kotov V.A., 1971. In: Howard R. (Ed.), Solar Magnetic Fields, Proc. 43rd IAU Symp., Reidel, Dordrecht, pp. 212–219.
Kuznetsov D.A., Kuklin G.V., Stepanov V.E., 1966. Rezul'taty nablyudenii i issledovanii v period MGSS, iss. 1, pp. 80–87. (In Russ.)
Livingston W.C., 1968. Astrophys. J., vol. 153, pp. 929–942.
Norton A.A., Jones E.H., Linton M.G., Leake J.E., 2017. Astrophys. J., vol. 842, iss. 1, article id. 3.
Pesnell W.D., Thompson B.J., Chamberlin P.C., 2012. Solar Phys., vol. 275, iss. 1–2, pp. 3–15.
Pevtsov A.A., Peregud N.L., 1990. Washington DC American Geophysical Union Geophysical Monograph Series, vol. 58, pp. 161–165.
Scherrer P.H., Schou J., Bush R.I., et al., 2012. Solar Phys., vol. 275, iss. 1–2, pp. 207–227.
Severnyi A.B., 1965. Sov. Astron., vol. 9, pp. 171–182.
Severny A.B., 1966. Astron. zhurn., vol. 43, pp. 465–479. (In Russ.)
Stepanov V.E., Severny A.B., 1962. Izv. Krymsk. Astrofiz. Observ., vol. 28, pp. 166–193. (In Russ.)